Biofabrication

International Society for Biofabrication

PAPER • OPEN ACCESS

Printability of pulp derived crystal, fibril and blend nanocellulose-alginate bioinks for extrusion 3D bioprinting

To cite this article: Zita M Jessop *et al* 2019 *Biofabrication* **11** 045006

Biofabrication

PAPER

Printability of pulp derived crystal, fibril and blend nanocellulose-alginate bioinks for extrusion 3D bioprinting

Zita M Jessop[1,2], Ayesha Al-Sabah[1,2], Neng Gao[1], Stuart Kyle[1], Bethan Thomas[3], Nafiseh Badiei[3], Karl Hawkins[3] and Iain S Whitaker[1,2]

[1] Reconstructive Surgery and Regenerative Medicine Research Group, Swansea University Medical School, Swansea, United Kingdom
[2] The Welsh Centre for Burns and Plastic Surgery, Morriston Hospital, Swansea, United Kingdom
[3] Centre for NanoHealth, Swansea University Medical School, Swansea, United Kingdom

E-mail: iainwhitaker@fastmail.fm

Keywords: nanocellulose, bioink, bioprinting, printability, rheology, nasoseptal chondrocyte

OPEN ACCESS

RECEIVED
16 August 2018

REVISED
24 January 2019

ACCEPTED FOR PUBLICATION
11 February 2019

PUBLISHED
8 July 2019

Abstract

Background: One of the main challenges for extrusion 3D bioprinting is the identification of non-synthetic bioinks with suitable rheological properties and biocompatibility. Our aim was to optimize and compare the printability of crystal, fibril and blend formulations of novel pulp derived nanocellulose bioinks and assess biocompatibility with human nasoseptal chondrocytes. *Methods:* The printability of crystalline, fibrillated and blend formulations of nanocellulose was determined by assessing resolution (grid-line assay), post-printing shape fidelity and rheology (elasticity, viscosity and shear thinning characteristics) and compared these to pure alginate bioinks. The optimized nanocellulose-alginate bioink was bioprinted with human nasoseptal chondrocytes to determine cytotoxicity, metabolic activity and bioprinted construct topography. *Results:* All nanocellulose-alginate bioink combinations demonstrated a high degree of shear thinning with reversible stress softening behavior which contributed to post-printing shape fidelity. The unique blend of crystal and fibril nanocellulose bioink exhibited nano- as well as micro-roughness for cellular survival and differentiation, as well as maintaining the most stable construct volume in culture. Human nasoseptal chondrocytes demonstrated high metabolic activity post printing and adopted a rounded chondrogenic phenotype after prolonged culture. *Conclusions:* This study highlights the favorable rheological, swelling and biocompatibility properties of nanocellulose-alginate bioinks for extrusion-based bioprinting.

1. Introduction

The ability to print biological 'inks' rather than traditional 3D printing of metals and plastic has resulted in the birth of the new bioprinting research field [1–4] which is gaining interest in engineering customized tissues for reconstructive surgery [5–7]. Developments in automative bioprinting technology, cell biology and material science has allowed production of an increasing range of 'printable' bioinks, consisting of cells and biocompatible materials, in an attempt to simultaneously replicate native tissue micro and macroarchitectures, overcoming the problems of repeatability and scalability of conventional tissue engineering strategies [6, 8].

Of the three-main 3D bioprinting technologies: extrusion, inkjet and laser-assisted, extrusion is the most versatile, fast, scalable and cost-effective [9, 10]. This technique relies on extruding bioinks with suitable mechanical properties (viscosity, elasticity, shear thinning) through a nozzle using either mechanical (piston or screw driven) or pneumatic forces. Suitable bioinks must also exhibit cellular viability, adhesion, proliferation and differentiation [8, 11]. Although it is easier to tailor the biomechanical properties of synthetic bioinks such as polyacrylamides and polyethylene glycols to suit extrusion techniques, their biocompatibility and tissue regenerative potential are inferior to non-synthetic bioinks such as gelatin, agarose, alginate, hyaluronic acid and collagen, which mimic the natural extracellular matrix environment [12].

Reconstruction of facial cartilage defects, from trauma, burns, skin cancer and congenital conditions, currently relies on using autologous grafts, most

commonly from the costochondral site [13], with significant donor site morbidity [14–17]. Current available tissue-engineered cartilage constructs, based on non-specific cell seeding of scaffolds, fail to replicate native tissue anisotropy [6, 18] and are therefore mechanically unstable [19–21] and prone to degradation [22, 23], calcification [18, 21] and inflammation *in vivo*, especially when synthetic biomaterials are used [24, 25], prompting research into non-synthetic alternatives.

Contemporary research into 3D bioprinting of cartilage has identified several potential natural bioinks, including fibrin, alginate, gelatin, Matrigel, and nanocellulose [26, 27], which have been used as scaffolds for facilitating cell homing from neighboring healthy tissue or deposition of extracellular matrix following the addition of cellular components such as chondrocytes or mesenchymal stem cells [28]. However, the application of the more commonly used bioinks can be a challenge due to suboptimal printability and pure alginate formulations, in particular, have been identified as providing poor post-printing shape fidelity even when viscosity is increased [8, 29].

Nanocellulose, a linear polysaccharide extracted from the biosynthesis of plants or bacteria, is an emerging class of advanced naturally derived nanomaterial. It is promising due to its attractive physicochemical properties, extraordinarily high stiffness (100–200 GPa) and strength, alongside its abundance and sustainability [30–32]. It is currently classified into three groups: (1) biomass-derived cellulose nanocrystals (CNC) (2) biomass-derived cellulose nanofibrils (CNF) and (3) bacterial nanocellulose (BNC) [10]. BNC has shown promise for tissue engineering applications due to its biocompatibility, nanostructure, functionalization potential, water-holding capacity and similarities in morphology to collagen, thereby providing cell support [33–42]. The unique biomechanical and rheological properties due to the high aspect ratio of bacterial cellulose have also meant that it has potential utility as a bioink for 3D bioprinting [10, 33, 43–47]. Compared to industrial scale production of CNF and CNC, obtained through chemical and mechanical treatment of biomass or wood pulp [32], the current techniques for producing BNC are limited by the huge substrate costs of supporting bacterial growth, low yield of products and concerns regarding residual bacterial toxins/epitopes, which has precluded widespread use [48–50].

There have been recent reports in the literature concerning pulp biomass derived CNC and CNF [27, 51, 52] bioinks which rely on 'top-down' NC extraction using an expensive enzymatic treatment step and concentrated acids with poor chemical recovery, making clinical translation and 'up-scaling' problematic [53–55]. A lower cost, scalable solution has presented itself in the form of American Value-Added Pulping (AVAP®) technology, using a tunable pre-treatment step without enzymes to produce CNF, CNC and a unique blend (NCB) formulation at low cost, high purity and with efficient, low cost chemical recovery [56]. Characterization of these formulations has revealed promising rheology for bioprinting and found that NCB exhibits porous fibrillar networks with interconnecting compact nanorods with favorable pore sizes for cellular ingress and maintenance [57]. This study optimizes pulp biomass derived CNF, CNC and NCB as bioinks for extrusion bioprinting and investigates their printability and biocompatibility using human nasoseptal chondrocytes.

2. Methods

2.1. Extrusion 3D bioprinting set up

A custom-built extrusion bioprinter with a variable speed control syringe driver mounted on a motor-driven XY-Z system featuring custom RepRap firmware was used to print 3D structures from NC/alginate hydrogel bioinks. Bioink was loaded into 5 ml syringes (Sterile BD Plastipak slip tip) and extruded through 610 μm precision nozzles (Adhesive Dispensing Ltd). Slic3r (open source software) allowed adjustment of print settings to suit the individual bioinks; including print-head movement speed, extrusion speed, layer height, infill pattern and density. The 3D model was sliced and exported as G-code to command the bioprinter. Initial calibration of the printer and software resulted in a minimum prefabrication 'single layer' of 1.7 mm to allow for continuous, uniform printing. Sterile printing was achieved in a class II laminar flow hood following cleaning of all external bioprinter components using 70% ethanol and UV treatment for 60 min.

2.2. Bioink preparation and optimization

2.2.1. Nanocellulose bioink production

Nanocellulose particles were produced as an aqueous slurry from raw wood chip biomass using patented AVAP® technology which fractionated biomass into cellulose, hemicelluloses and lignin using ethanol and sulfur dioxide, with morphology controlled by the time and temperature of the pre-treatment step [56, 57] (figure 1). The final nanocellulose formulations; hydrophilic BioPlus CNCs gel (pure cellulose, wt. 3%), hydrophilic BioPlus CNFs gel (wt. 6%) and hydrophilic BioPlus Blend gel (NCB, wt. 3%) consist of their respective nanocellulose particles and water.

CNC, NCB, and CNF were centrifuged at 1500G for 5 min to remove any residual bleaching chemicals and lignin fragments and steam sterilized in an autoclave (100 kPa, 121 °C, for 30 min). Alginic acid sodium salt (medium viscosity from brown algae, Sigma-Aldrich, Poole, UK) was UV sterilized for one hour prior to being dissolved in sterile culture medium to make up 0.625%, 1.25%, 2.5%, 5%, 7.5% and 10% alginate concentrations (w/v). One part alginate was combined with four parts nanocellulose (to create CNC-AG, NCB-AG and CNF-AG bioinks) as

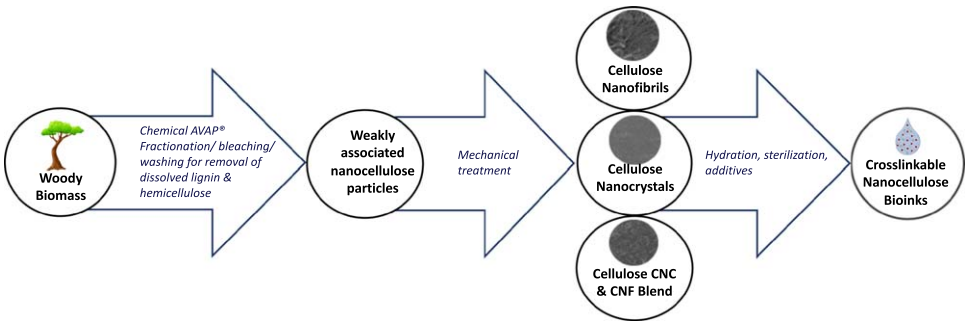

Figure 1. Process route for nanocellulose bioink production from wood pulp biomass.

Table 1. Alginate bioink additive qualitative analysis. Alginate concentrations were assessed against ease of dissolution, flow and mixing with nanocellulose blend (NCB) at room temperature and uncrosslinked post printing construct stability. Very easy (++++), easy (+++), average (++), difficult (+), not possible (−).

Alginate concentration (wt%)	Ease of dissolution	Ease of flow	Ease of mixing with NCB	Uncrosslinked printed construct stability
0.625	++++	++++	++++	Unstable
1.25	++++	++++	++++	Unstable
2.5	+++	+++	+++	Good
5	++	++	++	Good
7.5	+	+	++	Very good
10	−	−	−	Untested

described by Markstedt *et al* [27] to allow crosslinking with calcium chloride ($CaCl_2$) following bioprinting. Alginate solutions from 0.625% to 10% were qualitatively assessed against four criteria set to define optimal bioink preparations; ease of dissolution, ease of flow at room temperature, ease of mixing with NC, and structural retention when printed with NC (table 1).

2.2.2. Crosslinking optimization

Different concentrations (0.1, 0.5, and 1 M) of aerosolized $CaCl_2$ solutions (anhydrous $CaCl_2$ powder Sigma-Aldrich, Poole, UK, dissolved in distilled water) were tested for crosslinking time (from print completion to cessation of structural changes on application of an indentation force). All solutions were sterilized and filtered by a 0.22 μm cell filter (Merck Millipore, Watford, UK) and stored in an incubator at 37 °C before use. Cylindrical constructs measuring 27 mm in diameter and 7 single layers (11.9 mm) in height were printed using alginate concentrations of 2.5% and 5% mixed with nanocellulose in 1:4 ratio respectively as described above. Crosslinking was performed by aerosolized $CaCl_2$ between each layer.

2.2.3. Transmission electron microscopy (TEM)

Each sample (2 mg) was dispersed in 5 ml of deionized water and sonicated for 30 min. After sonication 50 μl of the sample was immediately taken and further dispersed into 1 ml of deionized water to prevent coalescence. This solution (10 μl) was added to 300 mesh copper grids coated with lacey carbon film. The grid was allowed to air dry prior to staining with a 1.5% uranyl acetate solution. For staining, a drop of the uranyl acetate solution was placed on a parafilm strip and the grid inverted onto the droplet for a few seconds. The samples were then allowed to air dry. Analysis was performed on a Jeol 2100 JEM operating at 200 KV.

2.3. Printability testing

2.3.1. Resolution

Print resolution using the three different formulations of NC (CNC-AG, CNF-AG and NCB-AG) was tested by printing 40 × 40 mm square grids a single layer tall (1.7 mm) with 27% rectilinear infill and crosslinked with 0.5 M $CaCl_2$ (figure 2), adapted from Markstedt *et al* [58]. Grid line thickness was measured at the halfway points of the infill diagonal lines using a digital caliper (figure 2(B)). Shape fidelity of bioprinted and crosslinked structures using the three formulations of NC (CNC-AG, CNF-AG and NCB-AG) was assessed by bioprinting 27 mm diameter cylinders with 7-layer height (11.9 mm) and measuring diameter and height immediate post-printing, at 24 and 72 h following immersion in culture media at 37 °C.

2.3.2. Shape fidelity

Complex structure testing utilized 3D geometrical shapes and anatomical STL models of auricular

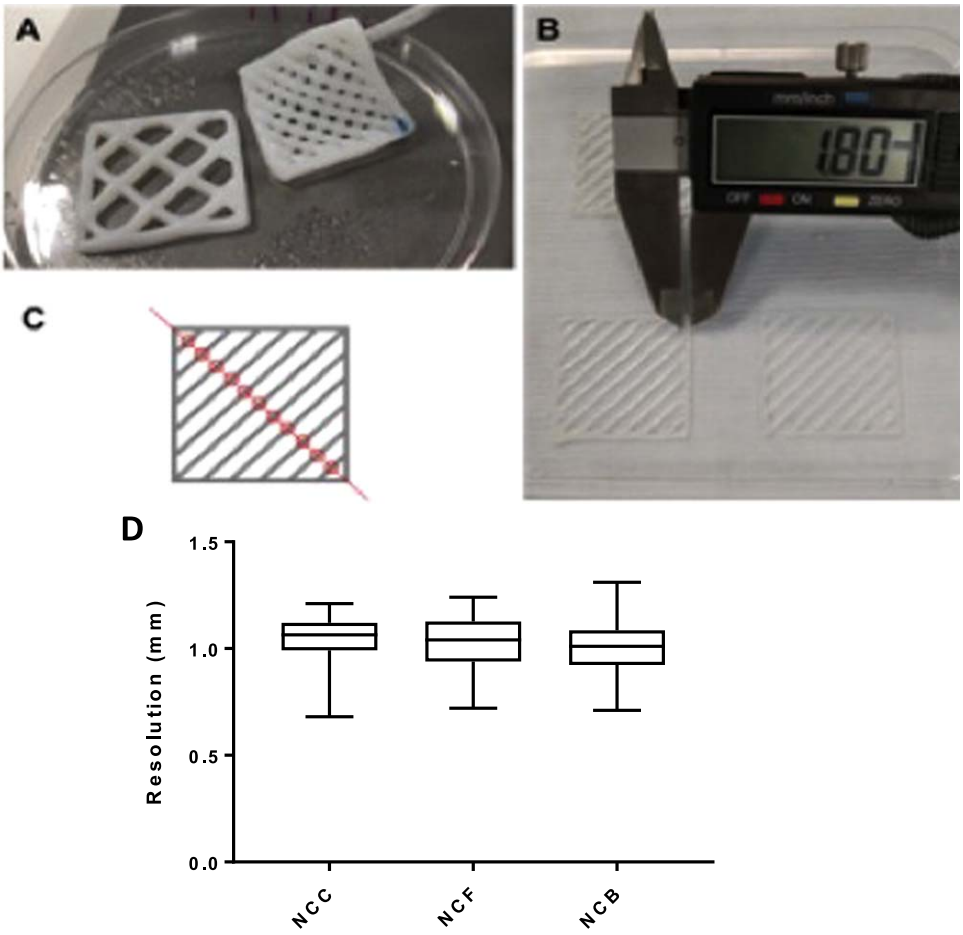

Figure 2. Grid thickness assay to testing bioprinting resolution for nanocellulose bioinks. (A) Crosslinked lattices printed using NCB-AG, showing structural retention on agitation with a spatula. (B) Electronic calliper measurement of filaments printed using NCB-AG. (C) Schematic diagram to illustrate measurement points of construct for resolution testing. (D) Filament thickness for CNC-AG, CNF-AG and NCB-AG formulations. Data is expressed as the mean, error bars indicate SD. Statistical differences was calculated by one-way ANOVA ($P = 0.424$, pooled data from four constructs, each with $N = 11$).

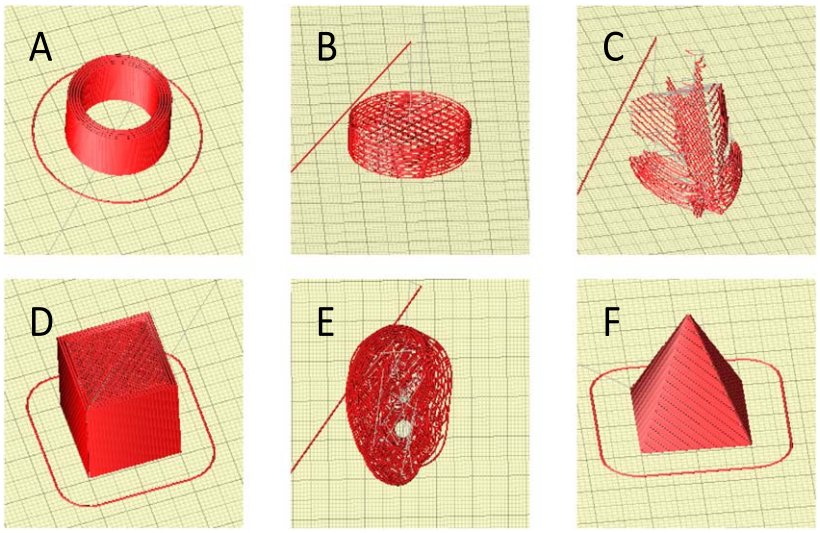

Figure 3. G-code in graphical format of the shapes used for complex structure testing. (A) Hollow cylinder, (B) cylinder, (C) nasal cartilage, (D) cube, (E) right ear, (F) 4-sided pyramid.

cartilage, obtained from an online open source repository, BodyParts3D© (The Database Center for Life Science, licensed under CC Attribution-Share Alike 2.1 Japan (http://lifesciencedb.jp/bp3d/) (figure 3). Cylindrical shapes were created using Microsoft 3D Builder software (Microsoft Corporation, New Mexico, USA) and exported in STL file format for 3D bioprinting. The volume was calculated by measuring the diameter ($2r$) and height (h) of the 3D printed cylindrical constructs using $V = \pi r2h$ to assess post printing shape fidelity after 24 and 48 h under culture conditions.

2.3.3. Rheology

The rheological properties of bioink mixtures (alginate 1.25%/2.5%/5% and NC mixtures with alginate 1.25%, 2.5% and 5% to create CNC-AG, NCB-AG and CNF-AG bioinks (with overall alginate concentrations of 0.25%, 0.5% and 1% (w/w) respectively) were measured using an AR-G2 (TA instruments, UK) Controlled Stress Rheometer fitted with a 40 mm diameter parallel plate geometry. Solutions were mixed on a rolling rocker for ~15 min before sample loading. Prior to each experiment, the zero gap was set on the rheometers and the geometry was calibrated using rotational mapping. Approximately 0.65 ml of sample was carefully loaded using a spatula onto the center of the lower plate of the rheometer and the upper plate was gradually lowered onto the sample until the gap was totally filled (gaps ranged from 350 to 500 μm). Any excess sample around the edge of the geometry was trimmed using a spatula. The normal force measured at the lower plate was set at a maximum of 0.1 N to ensure that any mechanical damage to the sample during gap setting procedure was minimized. The rheometers lower plate was controlled at a temperature of 22 °C and a low viscosity silicon oil (Fisher Scientific: Brookfield, Viscosity standard 0.920 specific gravity silicone oil 5 mPa s—Ref: 10543108) was used to surround the outer edges of the sample, in order to reduce sample evaporation.

Following a sample equilibration period of 2 min, a frequency sweep (0.1–10 Hz) was performed at a constant stress of 0.5 Pa. Each measurement was within the linear viscoelastic range of the sample as confirmed by stress sweeps (data not shown). The values of storage modulus (G') and loss modulus (G'') were recorded over the entire frequency range employed. Following the completion of the frequency sweep, the sample was allowed to equilibrate for a period of 10 s before a shear flow ramp was carried out over logarithmically increasing shear rates from 0.1 to 100 s^{-1} for a period of 2 min. Both frequency sweep and shear flow ramp experiments were repeated at least three times for each sample.

Table 2. Optimization of crosslinking with different $CaCl_2$concentrations. Quantitative analysis of crosslinking time (min) and qualitative analysis of crosslinking strength. Crosslinking strength defined by ability to withstand mechanical indent pressure: very light pressure (−), light pressure (+), moderate pressure (++).

$CaCl_2$ concentration (M)	Alginate concentration (wt%)	Crosslinking time (min)	Crosslinking strength
0.1	2.5	4	−
	5	4	−
0.5	2.5	2	+
	5	2	+
1	2.5	0 (Immediate)	+
	5	0 (Immediate)	++

2.4. 3D bioprinting with human nasoseptal chondrocytes

2.4.1. Cell culture, encapsulation and bioprinting

Chondrocytes were isolated from human nasoseptal cartilage samples obtained after informed consent (IRAS ID 99202) during routine septorhinoplasties. Cartilage tissue was minced into 1 mm^3 pieces and digested by 0.4% pronase (Roche, West Sussex, UK) at in culture media for 1 h at 37 °C (5% CO_2) with gentle agitation, followed by digestion with 0.2% collagenase type I for 18 h [59]. The solution was filtered through a 40 μm cell strainer (VWR, Leicestershire, UK) and then centrifuged at 500G for 5 min to replace the enzyme mixture with culture media. Cells were grown in 5% CO_2 at 37 °C and culture medium was changed every 2–3 d. Culture medium used consisted of Dulbecco's Modified Eagle Medium without glucose (Sigma-Aldrich, Poole, UK) supplemented with 10% fetal bovine serum (Sigma-Aldrich, Poole, UK), 100 μg ml^{-1} penicillin and 100 U ml^{-1} streptomycin (Sigma-Aldrich, Poole, UK), 1 mM glucose (Sigma-Aldrich, Poole, UK), and 0.1% non-essential amino acids (Thermo Fisher Scientific, Paisley, UK). Cells were passaged using 0.05% trypsin-EDTA (Thermo Fisher Scientific, Paisley, UK) when they reached 80%–90% confluency. The number of total and viable cells was estimated by 0.4% trypan blue staining using the Invitrogen™ Countess™ II automated cell counter (Thermo Fisher Scientific, Paisley, UK).

Passages 5–7 were chosen for subsequent experiments because it yielded the adequate number of chondrocytes for extrusion 3D bioprinting using 2×10^6 cells ml^{-1} of bioink [60]. Immediately prior to bioprinting of cell-laden bioinks, cell suspensions were drawn up into a syringe and gently mixed with a syringe of NC/Alginate bioink using a two-way tap under sterile conditions for one minute to ensure uniform distribution. Immediately post printing the cell-bioink constructs were washed in culture medium to remove the excess $CaCl_2$ before culturing in the incubator.

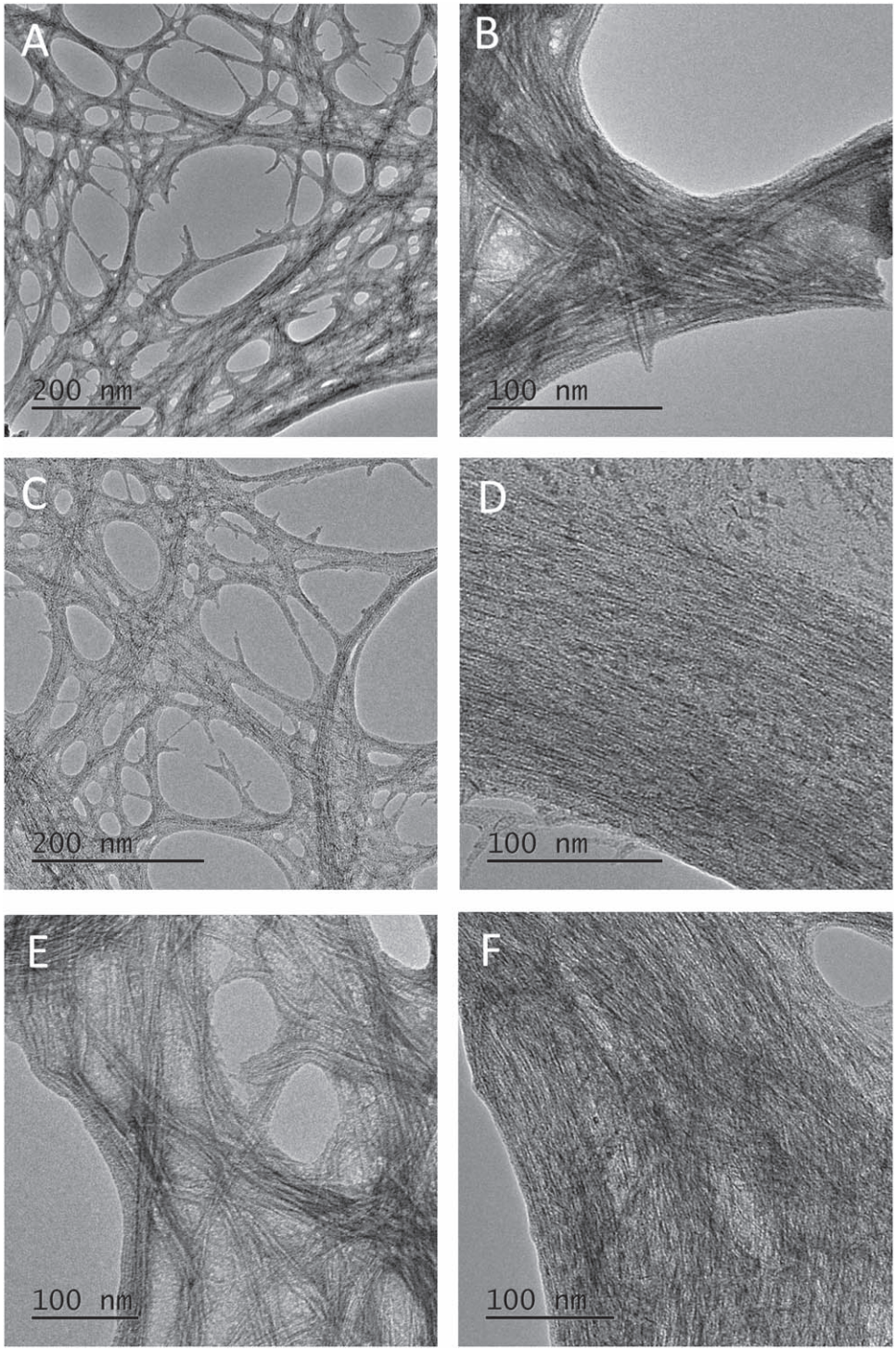

Figure 4. Transmission electron microscopy of nanocellulose-alginate bioinks before and after crosslinking. CNC-AG (A) and (B), CNF-AG (C) and (D) and NCB-AG (E) and (F) before (A), (C), (E) and after crosslinking with 0.5 M CaCl2 (B), (D), (F).

2.4.2. Biocompatibility

A LIVE/DEAD® Cell Viability Kit (Thermo Fisher Scientific, Paisley, UK) was used for assessment of cell viability according to the manufacturer's instructions at 24 and 48 h after bioprinting. The samples were stained with 2 μM calcein AM (green) and 1 μM ethidium homodimer-1 (red). Labeling was examined using confocal microscopy (Zeiss LSM 710 inverted confocal microscope), where green labeled cells represented live cells and red labeling indicated dead cells. Images were taken from at least six different areas of three bioprinted constructs for each condition, the number of live and dead cells were counted using NIH ImageJ software, and cell viability was then expressed as the percentage of the number of live cells to total cells.

Cell metabolic activity was quantified using 10% (v/v) AlamarBlue® cell viability reagent (Thermo Fisher Scientific, Paisley, UK) at 4, 12 and 24 h after bioprinting. The fluorescence was measured (at 530–560 nm excitation wavelength and 590 nm

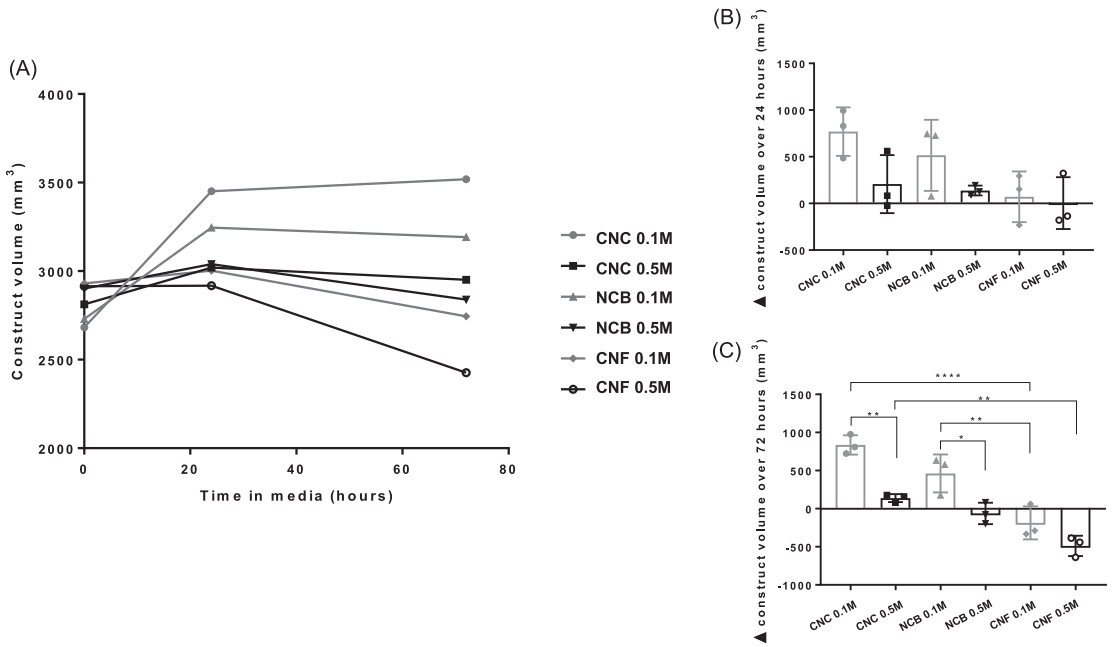

Figure 5. Bioprinted construct swelling properties. Comparison cylindrical construct volume bioprinted using three different bioink formulations (CNC-AG, NCB-AG and CNF-AG) crosslinked with either 0.1 M or 0.5 M $CaCl_2$ (A). Change in construct volume relative to time 0 at 24 (B) and 48 (C) hours. Data is expressed as the mean±SD ($N = 3$ for all groups). Statistical differences calculated by one-way ANOVA with Tukey's multiple comparison post-hoc test. $^{*}P < 0.05$, $^{**}P < 0.01$, $^{**}P < 0.001$.

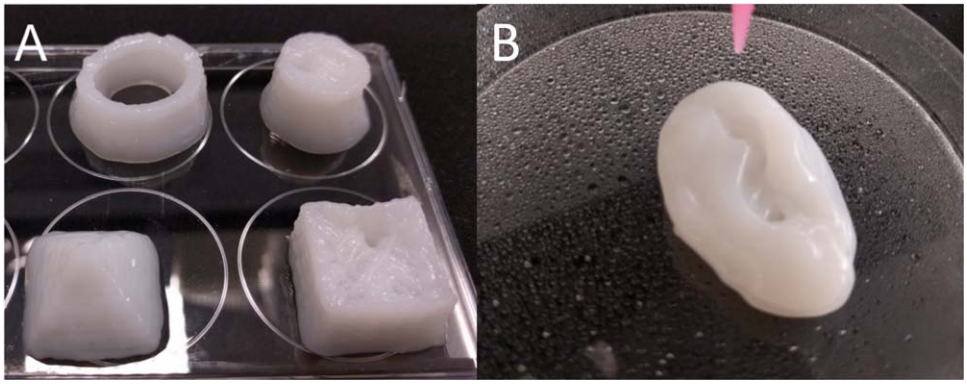

Figure 6. Nanocellulose bioinks for bioprinting complex structures. (A) Geometric structures printed using NCB-AG for complex shape testing; hollow cylinder (top left), cylinder (top right), pyramid (bottom left), and cube (bottom right). (B) Right ear.

emission wavelength) with plate reader (POLARstar Omega spectrophotometer, BMG LABTECH, Ortenberg, Germany). Matched concentration of cells in media were used as controls. The cross reactivity of Alamar Blue with nanocellulose in the medium was also tested. The OD values were normalized against that at $t = 0$. The cell viability was determined by plotting fluorescence emission intensity versus cell concentration.

2.4.3. Cytotoxicity

Cytotoxity of NCB bioink was assessed using lactose dehydrogenase (LDH) cytotoxicity assay. The plate containing cells with NCB-AG ($n = 6$) as well as cells only ($n = 6$), media only ($n = 3$) and NC controls ($n = 3$) were incubated at 37 °C, 5% CO_2 overnight. Then 50 μl of each sample medium was transferred to a 96-well plate and mixed with 50 μl Reaction Mixture for 30 min at room temperature, protected from light, at which point Stop Solution was added. The absorbance measurements (at 490 and 680 nm) was used to determine LDH activity.

2.4.4. Scanning electron microscopy (SEM)

Bioprinted and crosslinked cellular constructs grown for 3 weeks in culture were washed three times with 50 mM Sodium Cacodylate-HCl Buffer solution (pH 7.2–7.4, SPI Supplies) at 10–20 min intervals to remove excess salt. The sample were fixed overnight in 2% Glutaraldehyde (Sigma Aldrich, UK) and

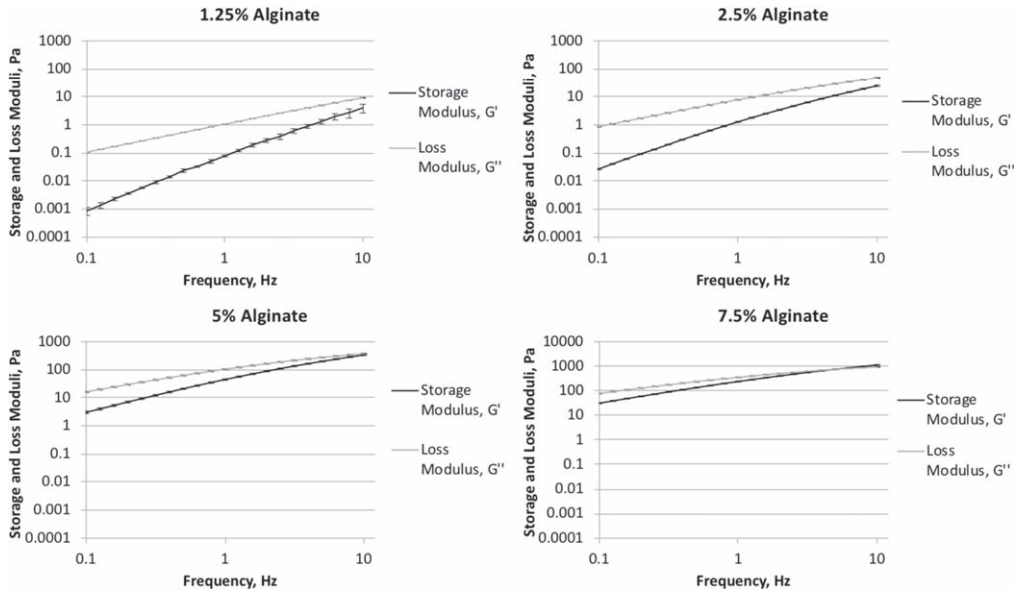

Figure 7. Rheological properties of pure alginate bioinks. G', storage moduli (dark gray); G'', loss moduli (light gray) for pure alginate bioink formulations at varying wt%, 1.25%, 2.5%, 5%, 7.5%. Data is expressed as the mean ±SD ($N = 5$ for all groups).

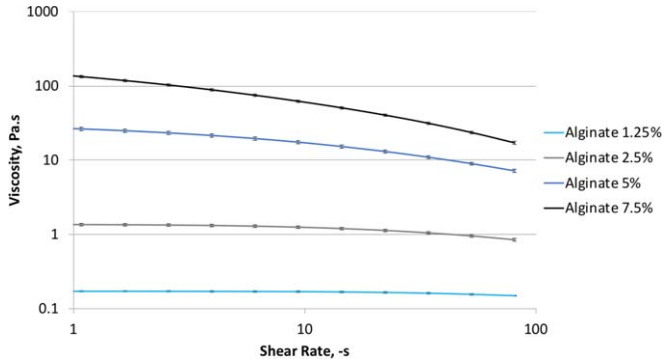

Figure 8. Viscosity of pure alginate bioinks as a function of shear rate. Data is expressed as the mean ±SD ($N = 5$ for all groups).

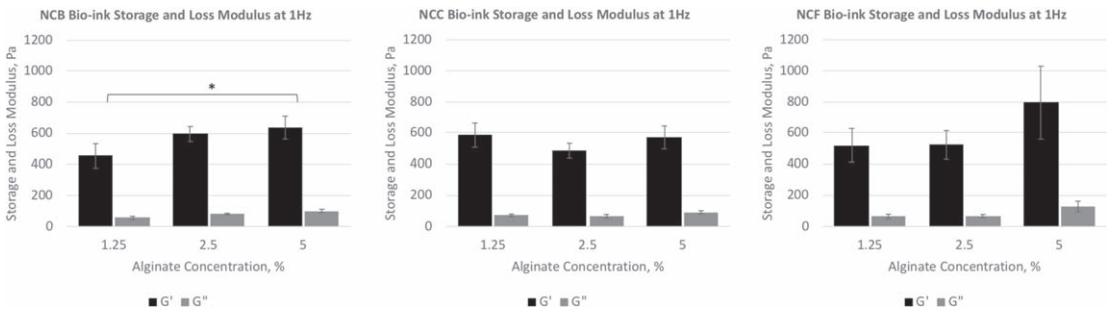

Figure 9. Rheological properties of nanocellulose-alginate bioinks at 1 Hz. G', storage moduli (dark gray); G'', loss moduli (light gray) for blend (NCB), crystal (CNC) and fibril (CNF) nanocellulose bioinks combined with 1.25%, 2.5% and 5% wt alginate. Data is expressed as the mean±SD ($N = 3$ for all groups). Statistical differences calculated by one-way ANOVA with Tukey's multiple comparison post-hoc test. $^{*}P < 0.05$.

dehydrated with a series of graded concentrations (30%–100%) of ethanol. The dehydrated sample was then rinsed with 50% hexamethyldisilazane solution (HMDS) in 100% ethanol for 10 min in a fume hood and then three times in 100% HMDS and left overnight to dry. The sample was coated with a thin layer of gold (~15 nm) using sputter coating and was imaged using SEM (Hitachi 4800s).

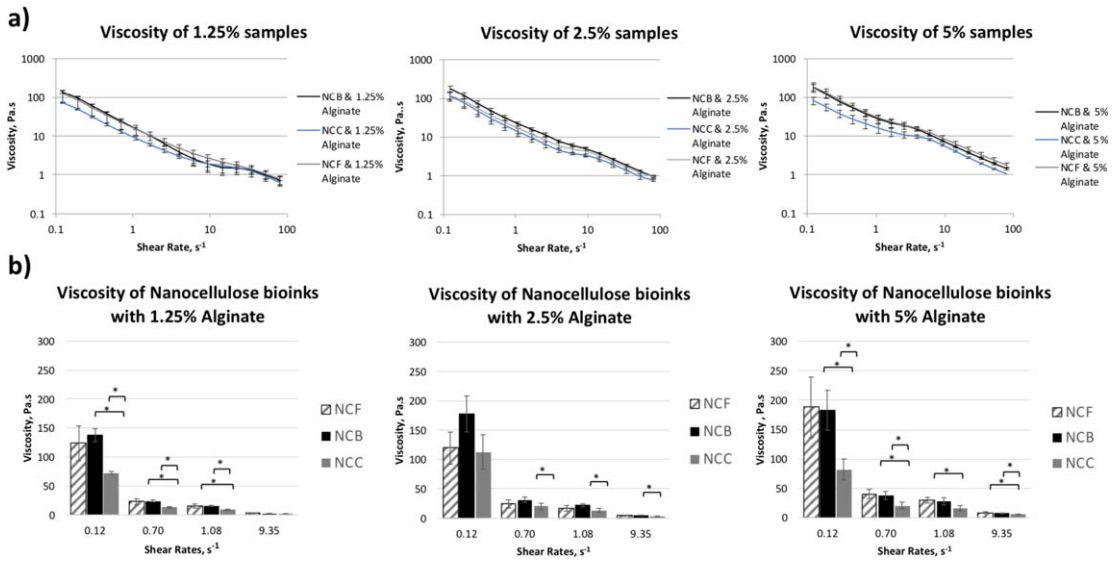

Figure 10. Viscosity for different nanocellulose-alginate bioinks as a function of shear rate. CNC, NCB and CNF bioinks combined with 1.25%, 2.5% and 5% alginate (AG). Data is expressed as the mean±SD ($N = 3$ for all groups). Statistical differences calculated using T-test's, $^{*}P < 0.05$.

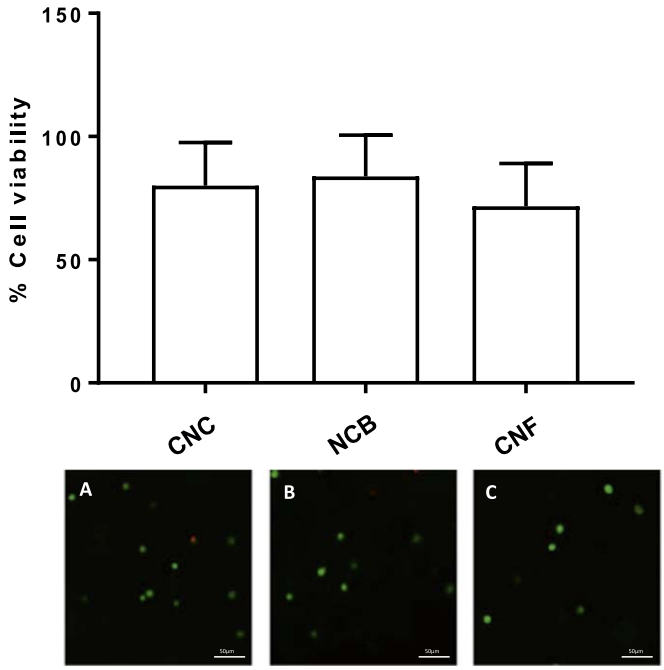

Figure 11. Human nasoseptal chondrocyte post bioprinting viability. Nanocellulose crystal; CNC-AG (A), blend; NCB-AG (B) and fibril; CNF-AG (C) bioink formulations. Data is expressed as the mean±SD ($N = 5$ for all groups). Statistical differences calculated by one-way ANOVA with Tukey's HSD multiple comparison post-hoc test ($P = 0.1502, N = 5$ with 3 biological repeats).

2.4.5. Compression testing

Mechanical tests were performed on bioprinted NCB-AG cylinder discs (5 mm diameter and 4 mm height), crosslinked with 0.5 M of $CaCl_2$ for 5 min and incubated in phosphate buffered saline (Thermo Fisher Scientific, Paisley, UK) at room temperature for 1 h to reach swelling equilibrium, using the BOSE ElectroForce® 3200 mechanical loading machine (Bose Corporation, ElectroForce® Systems Group, Minnesota, USA). The compressive strength of the samples was tested at 1 Hz. The compression (mm) and load (N) were recorded and Young's modulus was determined as the slope of the linear region of the stress/strain curve:

$$\text{Young's Modulus}(\text{N m}^{-2}\text{or Pa}) = \text{Stress}(\text{Pa})/\text{Strain}.$$

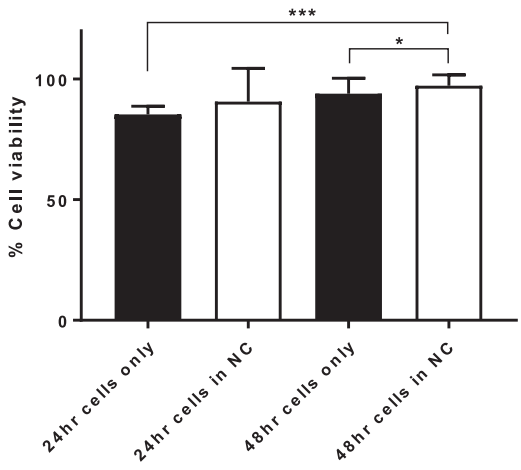

Figure 12. Human nasoseptal chondrocyte viability in 2D versus 3D culture in nanocellulose blend bioink. Viability post bioprinting with NCB-AG after 24 and 48 h in culture (white bars) versus 2D culture after 24 and 48 h (black bars). Data is expressed as the mean±SD ($N = 4$ for all groups). Statistical differences calculated by Mann–Whitney test. $^{*}P < 0.05$, $^{***}P < 0.001$.

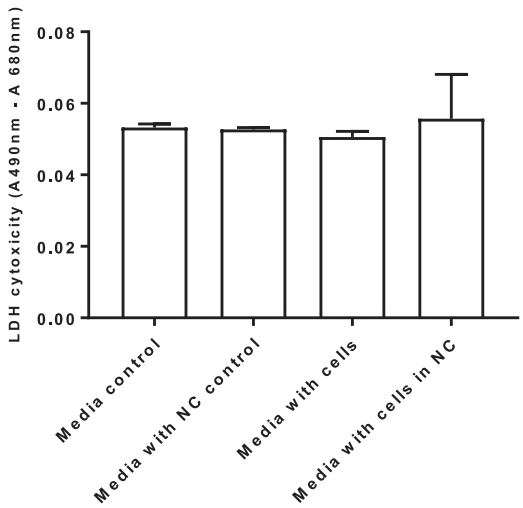

Figure 13. Lactate dehydrogenase (LDH) cytotoxicity assay. Cytotoxicity analysis of human nasoseptal chondrocytes in 2D culture versus post bioprinting with NCB-AG. Data is expressed as the mean ±SD. Statistical differences between media with cells and NCB-AG was calculated by Unpaired t test ($P = 0.322, N = 3$–6).

2.5. Statistical analysis

Quantitative results are expressed as mean ± standard deviation (SD), and the statistical analyses were performed using the GraphPad Prism 6.0 (GraphPad Software, La Jolla, CA, USA). Statistical analyses for single comparisons were performed using the Mann-Whitney U test for non-Gaussian distributions and the t test for Gaussian distribution. Multiple comparisons were performed by one-way ANOVA, followed by a Tukey's post hoc test. Number of biological replicates are indicated in each figure legend. A value of $p < 0.05$ was considered statistically significant.

3. Results

3.1. Nanocellulose bioink formulation and crosslinking optimization

0.625% alginate solution exhibited superior properties with regards to dissolution and mixing but quickly collapsed at room temperature post printing. 7.5% and 10% alginate solutions were difficult to dissolve and too viscous to mix evenly with NC. Concentrations 1.25%, 2.5% and 5% were found to have promising viscosities and mixing potential and went on to rheological testing. Optimum alginate concentration 2.5% was chosen for further experiments due its ability to balance ease of dissolution and mixing with uncrosslinked structure stability post printing (table 1).

Crosslinking optimization is summarized in table 2. 1 M $CaCl_2$ was crosslinked in the shortest time (immediately, compared to 2 min for 0.5 M and 4 min for 0.1 M), with final constructs able to withstand larger mechanical force compared to 0.5 and 0.1 M. However, it was found that the immediate crosslinking time of 1 M $CaCl_2$ resulted in crosslinking of the filament during deposition, causing dragging and ultimately spoiling the final printed structure. Figure 2(A) illustrates crosslinked lattice structures using 0.5 M $CaCl_2$ withstanding agitation using a spatula.

All three formulations displayed varying degrees of nanofiber entanglements and extensive porous networks as seen on TEM prior to crosslinking due to agglomeration (figures 4(A), (C), (E)) as reported in other studies [61]. NCB-AG shows fibrillar entanglements of NC nanofibrils interspersed with CNCs (figure 4(E)). On crosslinking with $CaCl_2$ the alginate pulls the nanofibrils and crystals together to reduce voids within the material and produce a firm structure that can be manipulated and withstand cell culture conditions (figures 4(B), (D), (F)).

3.2. 3D bioprinting of macrostructures using nanocellulose bioinks

NCB-AG had the highest resolution demonstrated by the median filament thickness of 1.01 mm compared to 1.07 mm and 1.04 mm for CNC-AG and CNF-AG respectively (figure 2(D)), however, this was not found to be statistically significant ($p = 0.42$, one-way ANOVA). Crosslinked CNC-AG and NCB-AG cylindrical constructs swelled, especially at low crosslinker concentrations, over 24 h under culture conditions (in media at 37 °C), but these changes were not statistically significant (figures 5(A) and (B)). After 72 h there was a significant increase in volume for CNC-AG (697.6 mm^3, p-value 0.003) and NCB-AG (523.9 mm^3, p-value 0.021) constructs crosslinked with 0.1 M versus 0.5 M $CaCl_2$ concentrations whereas constructs printed using CNF-AG decreased in volume, with 0.5 M crosslinked constructs having a greater reduction

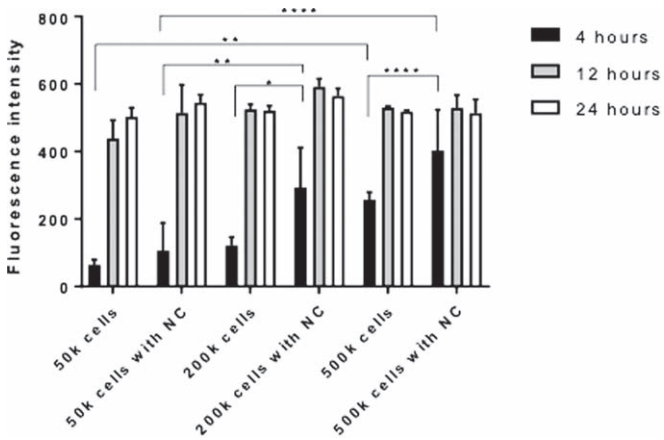

Figure 14. Metabolic activity of human nasoseptal chondrocytes in NCB-AG at 4, 12 and 24 h. The graph shows the fluorescence signal caused by reduction of alamarBlue (with the medium or medium plus NC value subtracted) in wells with increasing numbers of cells. Data is expressed as the mean±SD ($N = 5$ for all groups). Statistical differences calculated by one-way ANOVA with Tukey HSD multiple comparison post-hoc test. $^{*}P < 0.05$, $^{**}P < 0.01$, $^{***}P < 0.001$, $^{****}P < 0.0001$.

in volume (488.3 mm^3) than 0.1 M crosslinked ones (186.8 mm^3) from their original size (figure 5(C)). NCB-AG constructs crosslinked with 0.5 M $CalCl_2$ were the most stable under culture conditions with a reduction of 62.3 mm^3 from its original size.

Since NCB-AG crosslinked with 0.5 M CaCl2 demonstrated the most stable construct volume under culture conditions this was the formulation chosen for complex shape testing, including hollow cylinders and anatomical auricular cartilage (figure 6) and biocompatibility experiments.

3.3. Rheological properties of pulp-derived nanocellulose enable bioprinting

Pure alginate bioinks showed increasing G' and G'' with increasing frequency (figure 7). The mean loss moduli (G'') were consistently higher than mean storage moduli (G') for all concentrations (1.25%, 2.5%, 5% and 7%) demonstrating a dominance of viscous over elastic properties in pure alginate bioinks (figure 7). Shear rate ramps were performed to investigate the flow properties of bioinks by measuring the viscosity as a function of increasing shear rate. This revealed limited shear thinning behavior at 5% and 7.5% and near Newtonian behavior at 1.25% and 2.5% concentrations of pure alginate bioinks over the entire shear rates studied (figure 8).

However, unlike alginate bioinks, the mean G' for all NC bioinks is greater than the G'' over all frequencies studied indicating a dominance of elasticity and demonstrating strong interconnecting networks between nanostructures (figure 9). Shear rate ramps were performed to investigate the flow properties of CNF-AG, CNC-AG and NCB-AG bioinks by measuring the viscosity as a function of increasing shear rate (figure 10(A)). All nanocellulose containing bioinks exhibited a higher degree of non-Newtonian, shear thinning (pseudoelastic behavior) compared to pure alginate bioinks. CNF-AG and NCB-AG formulations demonstrated greater and statistically different viscosities compared to all CNC formulations. This difference is best seen at shear rate = 0.12 s^{-1} but is still present at higher shear rates (figure 10(B)). This implies that there are stronger particle–particle interactions or increased entanglements between nano- and microstructures within the NCB-AG and CNF-AG compared to CNC-AG bioinks, providing better shape fidelity post printing [27].

3.4. Nanocellulose is biocompatible with human nasoseptal chondrocytes

Immediately following bioprinting, cell viability was highest for NCB-AG (83.9% ± 16.7% live cells), followed by CNC-AG (80.1% ± 17.4%) and lastly CNF-AG (71.6% ± 17.4%) but differences were not statistically significant ($P = 0.1502$) (figure 11).

Constructs bioprinted using NCB-AG and crosslinked with 0.5 M $CaCl_2$ demonstrated the greatest volume stability and favorable cell viability and was therefore used for further biocompatibility experiments. Cell viability in NCB-AG (90.1% ± 13.8%) after 24 h in culture was comparable to cells on tissue culture plastic alone (85.3% ± 3.4%). However, by 48 h cell viability was significantly higher for cells cultured in NCB-AG (97.3% ± 4.5%) compared to cells on cultured on plastic alone (94.0% ± 6.4%, $P = 0.0326$) (figure 12).

Median LDH activity, an indicator of cytotoxicity, was not found to be significantly different between cells cultured on plastic versus bioprinted and cultured 3D in NCB-AG (0.05 versus 0.049 respectively, $P = 0.1138$) (figure 13). Human nasoseptal chondrocytes had significantly increased metabolic activity between 4 and 12 h in culture at all cell densities and conditions tested ($P < 0.0001$) but not between 12 and 24 h (figure 14). Chondrocytes demonstrated significantly increased

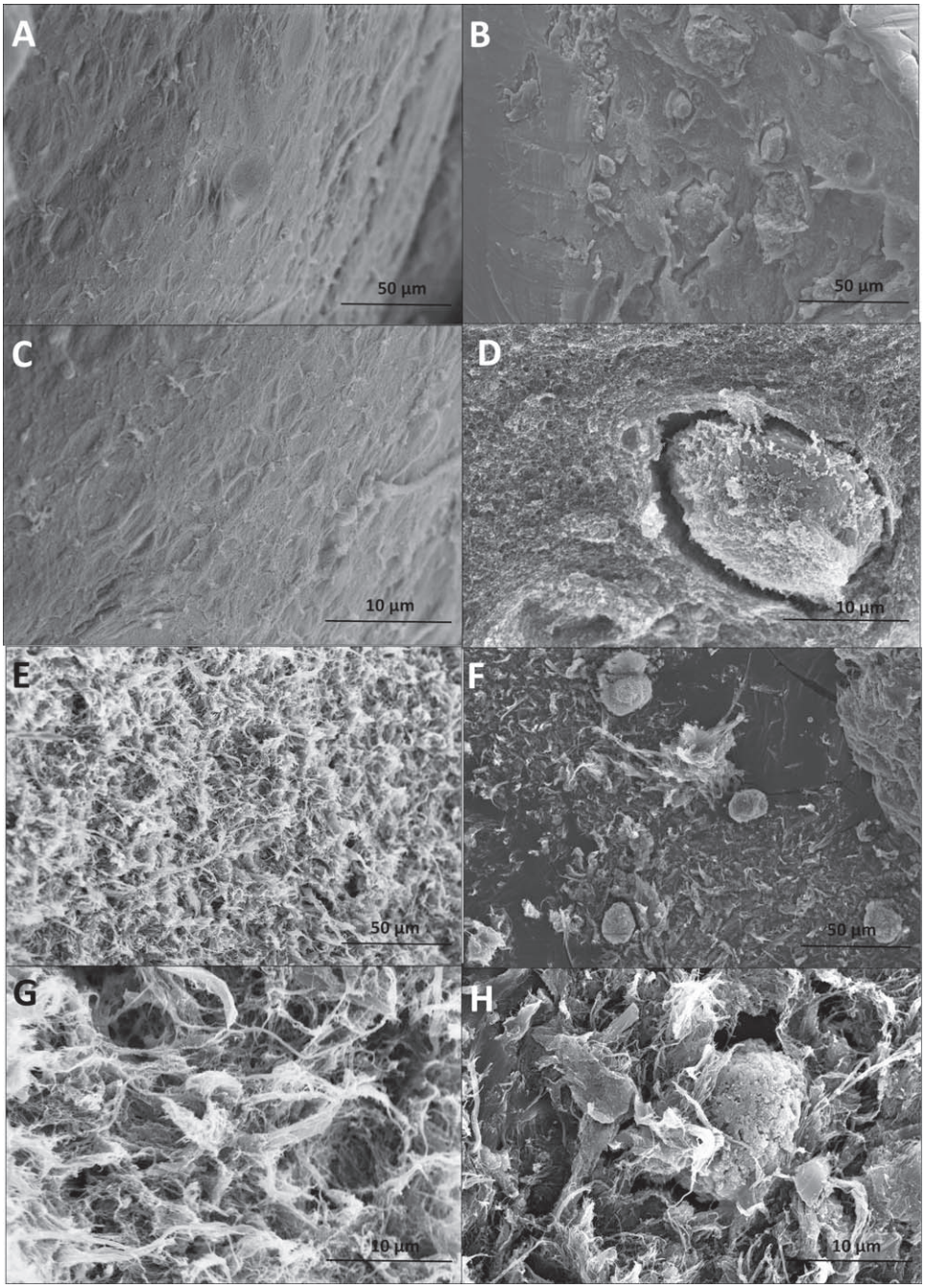

Figure 15. Scanning electron microscopy (SEM) of alginate and nanocellulose constructs following bioprinting. Alginate (A) and (C) and NCB-AG (E) and (G) bioinks without cells and alginate (B) and (D) and NCB-AG (F) and (H) bioinks after 21 d in culture with human nasoseptal chondrocytes, Scale bar (A), (B), (E), (H) is 50 μm and (C), (D), (G), (H) is 10 μm.

metabolic activity in NCB-AG compared to culture in 2D on plastic after four hours as measured by the fluorescence intensity for 2×10^5 (122.2 ± 23.9 versus 293.0 ± 118.1 respectively, $P = 0.0005$) and 5×10^5 (257.8 ± 21.0 versus 403.0 ± 120.5 respectively, $P = 0.0068$) cells (figure 14). At 12 and 24 h, the differences between the conditions are no longer significant.

SEM images demonstrate the relatively homogenous nature of 2.5% alginate bioink (figures 15(A) and (C)) compared to the highly porous structure of nanocellulose blend bioink consisting of varied nano and micro architecture, providing a larger surface area for cell adhesion (figures 15(E) and (G)). Human nasoseptal chondrocytes maintain a rounded cell morphology in both pure alginate (figures 15(B) and (D)) and nanocellulose blend (figures 15(F) and (H)) after 3 weeks in culture. Unconfined compression testing of bioprinted NCB-AG constructs crosslinked with 0.5 M $CaCl_2$ demonstrated a compressive/Young's Modulus of 52.6 kPa (figure 16).

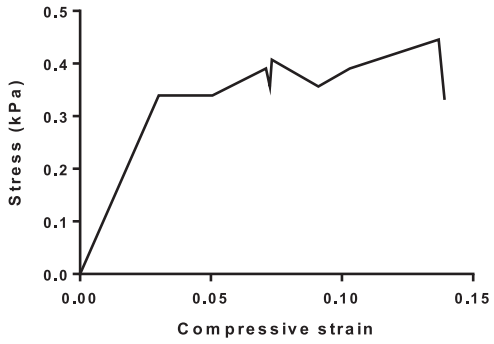

Figure 16. Stress strain curve for bioprinted constructs. Unconfined compression testing of bioprinted NCB-AG constructs crosslinked with 0.5 M $CaCl_2$ demonstrated a compressive/Young's modulus of 52.6 kPa.

4. Discussion

Nanocellulose is rapidly gaining interest for biomedical applications due to its unique physical, chemical and biological properties [50]. Results demonstrate that our optimized crystal, fibril and blend nanocellulose-alginate bioink formulations have comparable resolution, suitable rheology and biocompatibility with human nasoseptal chondrocytes to enable utility for cartilage bioprinting using extrusion-based techniques. The unique blend nanocellulose-alginate bioink (2.5% alginate, crosslinked with 0.5 M $CaCl_2$) offers the advantages of exhibiting nano- as well as microroughness for cellular functionality, as well as maintaining the most stable construct volume, to more reliably maintain the shape of patient specific cartilage constructs under culture conditions in the future. It was therefore chosen as the optimum bioink for our metabolic and topographical studies.

The few studies investigating bioprinting with pulp based nanocellulose have assessed crystal or fibril formulations individually [27, 51, 62] with none directly comparing CNC, NCB and CNF. Our previous work has demonstrated that AVAP technology produces nanocellulose with promising pore and fiber networks for tissue engineering applications [57]. TEM and SEM data in this study shows that even with addition of alginate all three NC formulations continue to be highly porous both in the nano and micro range, unlike pure alginate bioinks which are typically only nanoporous (approx. 5 nm) [63]. NCB hydrogels exhibited a combination of fibrillar networks and interconnecting compact nanorods and have been shown to have a broader variation in pore sizes (55 nm to over 12 μm, mean 934 nm) compared to those from CNC alone, which would allow chondrocyte migration (approx. 10 μm diameter) and provide a tunable nanotopography for a greater variety of bioactive signals [57].

The addition of alginate to allow crosslinking capability did not adversely affect the elasticity or shear thinning behavior of nanocellulose bioinks, which depends on the dry content of the ink rather than the ratio between the two components [27]. The storage modulus was greater than the loss modulus for all combinations of nanocellulose-alginate bioinks, over all frequencies studied, and therefore dominance of elasticity similar to pure nanocellulose materials [57]. This was in contrast to pure alginate bioinks, which are predominantly viscous. The large aspect ratio and ability to form interconnected network structures through hydrogen bonding makes nanocellulose both stiff due to the ordered (crystalline) regions and flexible due to the disordered (amorphous) regions of the nanoparticle [50]. These nanocellulose network structures can disentangle and align parallel to the direction of flow when placed in suspension which also accounts for the high degree of shear thinning exhibited in our study and has also been confirmed for other types of nanocellulose formulations in the literature [27, 62, 64]. Shear thinning enables bioprinting through fine deposition nozzles at low shear rates with reduced mechanical forces exerted on cells [27]. This is in contrast to the more commonly used pure alginate bioinks, which exhibit only limited shear thinning even at high shear rates requiring higher forces (shear stress) for extrusion which can impact post-printing cell viability [65–67]. Reversible stress softening behavior of nanocellulose means that post printing the storage modulus (G') is recovered under static conditions and is higher than that for pure alginate bioinks (in the 1.25%–7.5% range) contributing to shape fidelity and preventing collapse of complex 3D bioprinted constructs [47]. The rigidity of NCB was significantly higher than for CNC but similar to CNF indicating that the double network hydrogel structure previously reported for NCB is not disrupted by the addition of alginate [57].

Nanocellulose is broadly considered to be biocompatible using *in vivo* animal studies of BNC demonstrating no foreign body reaction or inflammation [68, 69]. Although it is well known that cellulose is not readily degraded by the human body due to the lack cellulolytic enzymes, non-enzymatic, spontaneous hydrolysis of cellulose chains have been suggested to account for slow breakdown which can be enhanced through oxidation [34, 70]. Even if not fully broken down, cellulose is biologically inert and theoretically should not interfere with homeostatic processes such as matrix remodeling [71]. Most reports on the nanotoxicology of nanocellulose use BNC and show no evidence of damage at the genetic, cellular and *in vivo* animal level [72] but few studies use human cells and none directly compare pulp based crystal, fibril and blend formulations [50]. Our study shows that pulp based nanocellulose is non-cytotoxic to nanoseptal chondrocytes with no significant differences in cell viability post-printing with CNC, NCB and CNF. NCB not only significantly increased the proportion of viable nasoseptal chondrocytes in culture after two days, it also encouraged them to be more metabolically active after the first four hours post

printing, whilst maintaining a rounded chondrogenic phenotype after three weeks in culture, suggesting a suitable 3D environment, nanotopography and porosity for cartilage matrix formation. These findings are consistent with previous studies indicating that maintenance of a round cell morphology is a prerequisite for overt chondrogenic differentiation [73]. The nanocellular fibrillary structures can mimic the properties of extracellular matrix components, which are also nanofibrillar networks composed of glycosaminoglycans and fibrous proteins, such as collagen, elastin, laminin and fibronectin, thereby encouraging cells to differentiate [74, 75]. The 3D bioprinted constructs themselves are immature and do not have the mechanical properties (Young's modulus 52.6 kPa) of native nasoseptal cartilage (in the region of 2–4 MPa [76]) and would require maturation via cartilage matrix secretion in a bioreactor before implantation to determine utility as cartilage tissue substitutes.

The AVAP process does not introduce post-hydrolysis modifications to the nanocellulose preparations which provides exiting potential for functionalization [56, 57]. The three available hydroxyl groups and negative surface charge allow the possibility of protein immobilization based on chemical conjugation and electrostatic adsorption respectively, in order to enhance cell attachment, migration, proliferation and differentiation [77].

5. Conclusion

3D bioprinting research has been gaining traction to transition from theory into practice and to ultimately allow biofabrication of customized and anatomically accurate replacement tissue using the patient's own cells for surgical reconstruction. Pulp derived nanocellulose was found to be extremely shear thinning with reversible stress softening behavior, thereby contributing to post-printing shape fidelity. The unique blend of crystal and fibril nanocellulose bioink exhibited nano- as well as micro-roughness for cellular survival and differentiation, as well as maintaining the most stable construct volume in culture. One of the major challenges in bioprinting any tissue type are bioinks that are printable, capable of maintaining complex macrostructures structures and able to provide an environment in which cells can thrive and differentiate, making pulp based nanocellulose a promising addition to the bioink research field.

Financial disclosure and products page

This work has been funded by the Welsh Clinical Academic Training Pathway (ZJ), ABM University Health Board/Health Research Wales (ISW), Oakgrove Foundation (ISW), Royal College of Surgeons of England (ZJ/ISW), British Association of Plastic and Reconstructive Surgeons (ZJ/ISW), Healing Foundation (NG), Medical Research Council (ZJ) [grant number MR/N002431/1], the Fulbright Commission (ZJ).

Data availability

The raw data required to reproduce these findings are available to download from [http://doi.org/10.17632/6cf8dv9bzw.1#file-93fd26ba-2dfc-49af-b322-79373744af74]. The processed data required to reproduce these findings are available to download from [http://doi.org/10.17632/6cf8dv9bzw.1#file-93fd26ba-2dfc-49af-b322-79373744af74].

ORCID iDs

Zita M Jessop https://orcid.org/0000-0003-2886-9165
Stuart Kyle https://orcid.org/0000-0001-9837-6863
Iain S Whitaker https://orcid.org/0000-0002-3922-2079

References

[1] Mironov V 2005 The second international workshop on bioprinting, biopatterning and bioassembly *Expert Opin. Biol. Ther.* **5** 1111–5
[2] Mironov V 2006 Toward Human Organ Printing: Charleston Bioprinting Symposium *ASAIO* **52** e27–30
[3] Derby B 2012 Printing and prototyping of tissues and scaffolds *Science* **338** 921–6
[4] Jakab K, Damon B, Neagu A, Kachurin A and Forgacs G 2006 Three-dimensional tissue constructs built by bioprinting *Biorheology* **43** 509–13
[5] Kamali P, Dean D, Skoracki R, Koolen P G, Paul M A, Ibrahim A M and Lin S J 2016 The current role of three-dimensional (3D) printing in plastic surgery *Plast. Reconstructive Surg.* **137** 1045–55
[6] Jessop Z M, Al-Sabah A, Gardiner M D, Combellack E, Hawkins K and Whitaker I S 2017 3D bioprinting for reconstructive surgery: principles, applications and challenges *J. Plast. Reconstructive Aesthetic Surg.* **70** 1155–70
[7] Thomas D J, Jessop Z M and Whitaker I S 2018 *3D bioprinting for reconstructive surgery: techniques and applications* 1st edn (Amsterdam: Elsevier)
[8] Kyle S, Jessop Z M, Al-Sabah A and Whitaker I S 2017 'Printability' of candidate biomaterials for extrusion based 3D printing: state-of-the-art *Adv. Healthcare Mater.* **6** 1–6
[9] Jakab K *et al* 2008 Tissue engineering by self-assembly of cells printed into topologically defined structures *Tissue Eng.* A **14** 413–21
[10] Piras C C, Fernandez-Prieto S and Borggraeve W M D 2017 Nanocellulosic materials as bioinks for 3D bioprinting *Biomater. Sci.* **5** 1988–92
[11] Katja H, Shengmao L, Liesbeth T, Sandra Van V, Linxia G and Aleksandr O 2016 Bioink properties before, during and after 3D bioprinting *Biofabrication* **8** 032002
[12] Suntornnond R, Tan E Y S, An J and Chua C K 2016 A mathematical model on the resolution of extrusion bioprinting for the development of new bioinks *Materials* **9** 756
[13] Yilmaz M, Vayvada H, Menderes A, Mola F and Atabey A 2007 Dorsal nasal augmentation with rib cartilage graft: long-term results and patient satisfaction *J. Craniofacial Surg.* **18** 1457–62

[14] Ohara K, Nakamura K and Ohta E 1997 Chest wall deformities and thoracic scoliosis after costal cartilage graft harvesting *Plast. Reconstructive Surg.* **99** 1030–6
[15] Long X, Yu N, Huang J and Wang X 2013 Complication rate of autologous cartilage microtia reconstruction: a systematic review *Plast. Reconstructive Surg. Glob. Open* **1** e57
[16] Wee J, Park M, Oh S and Jin H 2015 Complications associated with autologous rib cartilage use in rhinoplasty: a meta-analysis *JAMA Facial Plast. Surg.* **17** 49–55
[17] Varadharajan K, Sethukumar P, Anwar M and Patel K 2015 Complications associated with the use of autologous costal cartilage in rhinoplasty: a systematic review *Aesthetic Surg. J.* **35** 644–52
[18] Bichara D A, O'Sullivan N A, Pomerantseva I, Zhao X, Sundback C A, Vacanti J P and Randolph M A 2012 The tissue-engineered auricle: past, present, and future *Tissue Eng.* B **18** 51–61
[19] Mark R H, Barbara L S, Robert L S and Deborah W 2002 Effects of serial expansion of septal chondrocytes on tissue-engineered neocartilage composition *Otolaryngology–Head Neck Surg.* **127** 398–408
[20] Nabzdyk C, Pradhan L, Molina J, Perin E, Paniagua D and Rosenstrauch D 2009 Auricular chondrocytes—from benchwork to clinical applications *In Vivo* **23** 369-80
[21] Kusuhara H, Isogai N, Enjo M, Otani H, Ikada Y, Jacquet R, Lowder E and Landis W J 2009 Tissue engineering a model for the human ear: assessment of size, shape, morphology, and gene expression following seeding of different chondrocytes *Wound Repair Regen.* **17** 136–46
[22] Cao Y, Vacanti J P, Paige K T, Upton J and Vacanti C A 1997 Transplantation of chondrocytes utilizing a polymer-cell construct to produce tissue-engineered cartilage in the shape of a human ear *Plast. Reconstructive Surg.* **100** 297–302 discussion 303–4
[23] Brommer H, Brama P A, Laasanen M S, Helminen H J, van Weeren P R and Jurvelin J S 2005 Functional adaptation of articular cartilage from birth to maturity under the influence of loading: a biomechanical analysis *Equine Vet. J.* **37** 148–54
[24] Christophel J, Chang J and Park S S 2006 Transplanted tissue-engineered cartilage *Arch. Facial Plast. Surg.* **8** 117–22
[25] Nayyer L, Patel K H, Esmaeili A, Rippel R A, Birchall M, O'Toole G, Butler P E and Seifalian A M 2012 Tissue engineering: revolution and challenge in auricular cartilage reconstruction *Plast. Reconstructive Surg.* **129** 1123–37
[26] Leppiniemi J, Lahtinen P, Paajanen A, Mahlberg R, Metsä-Kortelainen S, Pinomaa T, Pajari H, Vikholm-Lundin I, Pursula P and Hytönen V P 2017 3D-printable bioactivated nanocellulose–alginate hydrogels *ACS Appl. Mater. Interfaces* **9** 21959–70
[27] Markstedt K, Mantas A, Tournier I, Martinez Avila H, Hagg D and Gatenholm P 2015 3D bioprinting human chondrocytes with nanocellulose-alginate bioink for cartilage tissue engineering applications *Biomacromolecules* **16** 1489–96
[28] Murphy S V and Atala A 2014 3D bioprinting of tissues and organs *Nat. Biotechnol.* **32** 773
[29] Jia J *et al* 2014 Engineering alginate as bioink for bioprinting *Acta Biomater.* **10** 4323–31
[30] Habibi Y, Lucia L A and Rojas O J 2010 Cellulose nanocrystals: chemistry, self-assembly, and applications *Chem. Rev.* **110** 3479–500
[31] Klemm D, Kramer F, Moritz S, Lindström T, Ankerfors M, Gray D and Dorris A 2011 Nanocelluloses: a new family of nature-based materials *Angew. Chem., Int. Ed.* **50** 5438–66
[32] Dufresne A 2013 Nanocellulose: a new ageless bionanomaterial *Mater. Today* **16** 220–7
[33] Martínez Ávila H *et al* 2015 Novel bilayer bacterial nanocellulose scaffold supports neocartilage formation *in vitro* and *in vivo Biomaterials* **44** 122–33
[34] Li J, Wan Y, Li L, Liang H and Wang J 2009 Preparation and characterization of 2,3-dialdehyde bacterial cellulose for potential biodegradable tissue engineering scaffolds *Mater. Sci. Eng.* C **29** 1635–42
[35] Grande C J, Torres F G, Gomez C M and Bañó M C 2009 Nanocomposites of bacterial cellulose/hydroxyapatite for biomedical applications *Acta Biomater.* **5** 1605–15
[36] Chen Y M, Tingfei X, Yudong Z, Tingting G, Jiaquan H, Yizao W and Chuan G 2009 *In vitro* cytotoxicity of bacterial cellulose scaffolds used for tissue-engineered bone *J. Bioact. Compat. Polym.* **24** 137–45
[37] Gatenholm P and Klemm D 2010 Bacterial nanocellulose as a renewable material for biomedical applications *MRS Bull.* **35** 208–13
[38] Petersen N and Gatenholm P 2011 Bacterial cellulose-based materials and medical devices: current state and perspectives *Appl. Microbiol. Biotechnol.* **91** 1277
[39] Rambo C R, Recouvreux D O S, Carminatti C A, Pitlovanciv A K, Antônio R V and Porto L M 2008 Template assisted synthesis of porous nanofibrous cellulose membranes for tissue engineering *Mater. Sci. Eng.* C **28** 549–54
[40] Klemm D, Schumann D, Udhardt U and Marsch S 2001 Bacterial synthesized cellulose—artificial blood vessels for microsurgery *Prog. Polym. Sci.* **26** 1561–603
[41] Dugan J M, Gough J E and Eichhorn S J 2013 Bacterial cellulose scaffolds and cellulose nanowhiskers for tissue engineering *Nanomedicine* **8** 287–98
[42] Nimeskern L, Martínez Ávila H, Sundberg J, Gatenholm P, Müller R and Stok K S 2013 Mechanical evaluation of bacterial nanocellulose as an implant material for ear cartilage replacement *J. Mech. Behav. Biomed. Mater.* **22** 12–21
[43] Torres-Rendon J G, Köpf M, Gehlen D, Blaeser A, Fischer H, Laporte L D and Walther A 2016 Cellulose nanofibril hydrogel tubes as sacrificial templates for freestanding tubular cell constructs *Biomacromolecules* **17** 905–13
[44] Backdahl H, Helenius G, Bodin A, Nannmark U, Johansson B R, Risberg B and Gatenholm P 2006 Mechanical properties of bacterial cellulose and interactions with smooth muscle cells *Biomaterials* **27** 2141–9
[45] Malm C J, Risberg B, Bodin A, Bäckdahl H, Johansson B R, Gatenholm P and Jeppsson A 2012 Small calibre biosynthetic bacterial cellulose blood vessels: 13-months patency in a sheep model *Scand. Cardiovascular J.* **46** 57–62
[46] Rosen C L, Steinberg G K, DeMonte F, Delashaw J J B, Lewis S B, Shaffrey M E, Aziz K, Hantel J and Marciano F F 2011 Results of the prospective, randomized, multicenter clinical trial evaluating a biosynthesized cellulose graft for repair of dural defects *Neurosurgery* **69** 1093–104
[47] Torres F G, Commeaux S and Troncoso O P 2012 Biocompatibility of bacterial cellulose based biomaterials *J. Funct. Biomater.* **3** 864–78
[48] Lee K Y, Buldum G, Mantalaris A and Bismarck A 2014 More than meets the eye in bacterial cellulose: biosynthesis, bioprocessing, and applications in advanced fiber composites *Macromol. Biosci.* **14** 10–32
[49] Svensson A, Nicklasson E, Harrah T, Panilaitis B, Kaplan D L, Brittberg M and Gatenholm P 2005 Bacterial cellulose as a potential scaffold for tissue engineering of cartilage *Biomaterials* **26** 419–31
[50] Lin N and Dufresne A 2014 Nanocellulose in biomedicine: current status and future prospect *Eur. Polym. J.* **59** 302–25
[51] Nguyen D *et al* 2017 Cartilage tissue engineering by the 3D Bioprinting of iPS cells in a nanocellulose/alginate bioink *Sci. Rep.* **7** 658
[52] Martínez Ávila H, Schwarz S, Rotter N and Gatenholm P 2016 3D bioprinting of human chondrocyte-laden nanocellulose hydrogels for patient-specific auricular cartilage regeneration *Bioprinting* **1-2** 22–35
[53] Pääkkö M *et al* 2007 Enzymatic hydrolysis combined with mechanical shearing and high-pressure homogenization for nanoscale cellulose fibrils and strong gels *Biomacromolecules* **8** 1934–41
[54] Kumar A, Negi Y S, Choudhary V and Bhardwaj N K 2014 Characterization of cellulose nanocrystals produced by acid-hydrolysis from sugarcane bagasse as agro-waste *J. Mater. Phys. Chem.* **2** 1–8

[55] Kumar A, Rao K M and Han S S 2018 Mechanically viscoelastic nanoreinforced hybrid hydrogels composed of polyacrylamide, sodium carboxymethylcellulose, graphene oxide, and cellulose nanocrystals *Carbohydrate Polym.* **193** 228–38
[56] Nelson K and Retsina T 2014 Innovative nanocellulose process breaks the cost barrier *Tappi J* **13** 19–23
[57] Kyle S *et al* 2018 Characterization of pulp derived nanocellulose hydrogels using AVAP® technology *Carbohydrate Polym.* **198** 270–80
[58] Markstedt T E *et al* 2015 3D bioprinting human chondrocytes with nanocellulose-alginate bioink for cartilage *Biomacromolecules* **16** 1489–96
[59] Oseni A O, Butler P E and Seifalian A M 2013 Optimization of chondrocyte isolation and characterization for large-scale cartilage tissue engineering *J. Surg. Res.* **181** 41–8
[60] Li X, Chen S, Jingchao L, Wang X, Zhang J, Kawazoe N and Chen G 2016 3D culture of chondrocytes in gelatin hydrogels with different stiffness *Polymers* **8** 269
[61] Kvien I, Tanem B S and Oksman K 2005 Characterization of cellulose whiskers and their nanocomposites by atomic force and electron microscopy *Biomacromolecules* **6** 3160–5
[62] Siqueira G, Kokkinis D, Libanori R, Hausmann Michael K, Amelia S G, Neels A, Tingaut P, Zimmermann T, Jennifer A L and André R S , 2017 Cellulose nanocrystal Inks for 3D printing of textured cellular architectures *Adv. Funct. Mater.* **27** 1604619
[63] Boontheekul T, Kong H J and Mooney D J 2005 Controlling alginate gel degradation utilizing partial oxidation and bimodal molecular weight distribution *Biomaterials* **26** 2455–65
[64] Ureña-Benavides E E, Ao G, Davis V A and Kitchens C L 2011 Rheology and phase behavior of lyotropic cellulose nanocrystal suspensions *Macromolecules* **44** 8990–8
[65] Jungst T, Smolan W, Schacht K, Scheibel T and Groll J 2016 Strategies and molecular design criteria for 3D printable hydrogels *Chem. Rev.* **116** 1496–539
[66] Zhang X and Zhang Y 2015 Tissue engineering applications of three-dimensional bioprinting *Cell Biochem. Biophys.* **72** 777–82
[67] Malda J, Visser J, Melchels Ferry P, Jüngst T, Hennink Wim E, Dhert Wouter J A, Groll J and Hutmacher Dietmar W 2013 25th anniversary article: engineering hydrogels for biofabrication *Adv. Mater.* **25** 5011–28
[68] Helenius G, Backdahl H, Bodin A, Nannmark U, Gatenholm P and Risberg B 2006 *In vivo* biocompatibility of bacterial cellulose *J. Biomed. Mater. Res.* A **76** 431–8
[69] Fábia K A, Nuno A, Irina A, Fátima G, Ana Colette M, Lúcia L A and Miguel G 2012 Studies on the biocompatibility of bacterial cellulose *J. Bioact. Compat. Polym.* **28** 97–112
[70] Czaja W K, Young D J, Kawecki M and Brown R M 2007 The future prospects of microbial cellulose in biomedical applications *Biomacromolecules* **8** 1–12
[71] Muller M, Ozturk E, Arlov O, Gatenholm P and Zenobi-Wong M 2017 Alginate sulfate-nanocellulose bioinks for cartilage bioprinting applications *Ann. Biomed. Eng.* **45** 210–23
[72] Jeong S I, Lee S E, Yang H, Jin Y-H, Park C-S and Park Y S 2010 Toxicologic evaluation of bacterial synthesized cellulose in endothelial cells and animals *Mol. Cell. Toxicol.* **6** 370–7
[73] Barna M and Niswander L 2007 Visualization of cartilage formation: insight into cellular properties of skeletal progenitors and chondrodysplasia syndromes *Dev. Cell* **12** 931–41
[74] Fernandes H, Moroni L, van Blitterswijk C and de Boer J 2009 Extracellular matrix and tissue engineering applications *J. Mater. Chem.* **19** 5474–84
[75] Bhattacharya M *et al* 2012 Nanofibrillar cellulose hydrogel promotes three-dimensional liver cell culture *J. Control. Release* **164** 291–8
[76] Griffin M F, Premakumar Y, Seifalian A M, Szarko M and Butler P E 2016 Biomechanical characterisation of the human nasal cartilages; implications for tissue engineering *J. Mater. Sci., Mater. Med.* **27** 11
[77] Kuzmenko V, Sämfors S, Hägg D and Gatenholm P 2013 Universal method for protein bioconjugation with nanocellulose scaffolds for increased cell adhesion *Mater. Sci. Eng.* C **33** 4599–607